

Highly efficient prism coupling to whispering gallery modes of a square μ cavity

Yong-Le Pan and Richard K. Chang^{a)}

Department of Applied Physics and Center for Laser Diagnostic, Yale University, New Haven, Connecticut 06520-8284

(Received 26 September 2002; accepted 2 December 2002)

By using prism coupling to a square μ cavity, over 75% energy transfer to the whispering gallery modes ($Q > 10^6$) by frustrated total internal reflection was observed. A good comparison was found between measured data and theoretical model (based on a Fabry–Perot resonator), for the dependence of the coupling and linewidth of the whispering gallery modes (WGMs) as a function of relative separation between the prism and the μ cavity. By selecting the incident angle at the prism interface, the coupling to all four different sets of WGMs can be changed to coupling to only one set of WGMs. © 2003 American Institute of Physics. [DOI: 10.1063/1.1540242]

Whispering gallery modes (WGMs) circulating in planar (two-dimensional) dielectric μ cavities (in the form of rings,^{1,2} circles,^{3–6} race-tracks,⁷ hexagons,^{8,9} and squares^{9–11}) are of particular interest to dense wavelength division multiplexing (DWDM) part of optical communications. By placing one or several coupled microrings between two nearby optical waveguides, it has been demonstrated that a spectrally narrow channel can be added or removed from the signal waveguides (add/drop filters).^{1,7} Most of the coupling between the waveguides and μ cavities is through the separation-dependent frustrated total reflection (FTR) of the waves. The critical coupling condition occurs when the internal loss of the μ cavity is equal to the waveguide coupling loss. At this critical condition, the transmission of the signal waveguide approaches zero at WGM wavelengths, where the round-trip phase shift of the circulating wave in the μ cavity is in phase with the incoming wave. Several input devices have been used to couple the light into the μ cavities: prism,^{8,10} angle polished fiber tips,³ half-block fiber couplers,⁴ tapered optical fibers,⁵ planar waveguides,^{1,2,7,9} and focused beam.¹¹ In order to increase the separation-dependent coupling between a straight-shaped input waveguide and the μ cavity, investigators have worked on other than curved-shaped μ cavity designs (i.e., race-track, hexagon, and square).

The square-shaped μ cavity has the property that all four-bounce ray orbits with 45° internal incident angle (θ_{inc}) have the same length and, hence, all the corresponding WGMs have the same wavelengths. At slightly different wavelengths, there can exist four-bounce ray orbits with $\theta_{\text{inc}} < 45^\circ$ (where θ_{inc} must be greater than the critical angle for total internal reflection, θ_c). After one round trip, these $\theta_{\text{inc}} < 45^\circ$ orbits are not closed, even though these orbits correspond to different sets of WGMs when they are in phase with the input wave.¹¹

In this letter, we show that a prism can efficiently couple (more than 75%), by FTR, to four different sets of WGMs that are circulating around a square-shaped fiber, which is the square μ cavity. We observed that the prism-fiber distance

for maximum coupling (d_{mc}) depends on the different sets of WGMs with their undercoupled Q values. By selecting θ_{inc} , the coupling to multi-WGMs can be changed to coupling mainly with one set of WGMs. The measured dependence on the prism-fiber distance (greater and less than d_{mc}) of the WGMs linewidth and transmitted intensity into the square resonator were in good agreement with existing theory for standard Fabry–Perot resonators.¹⁰

A schematic of the experimental arrangement is shown in Fig. 1. A tunable external-cavity diode laser (with a linewidth of 300 kHz around 672 nm) beam was focused to a spot (size $\sim 30 \mu\text{m}$) on the hypotenuse of a 90° prism (*SF11*, refractive index $n_1 = 1.785$). The laser beam was 45° linearly polarized and thus TE or TM mode can be investigated by using two polarizers (for the input and output radiation) with the electric vector either perpendicular or parallel to the fiber axis. Two photodiodes (*D1* and *D2*) were used to monitor the input intensity and the remaining re-

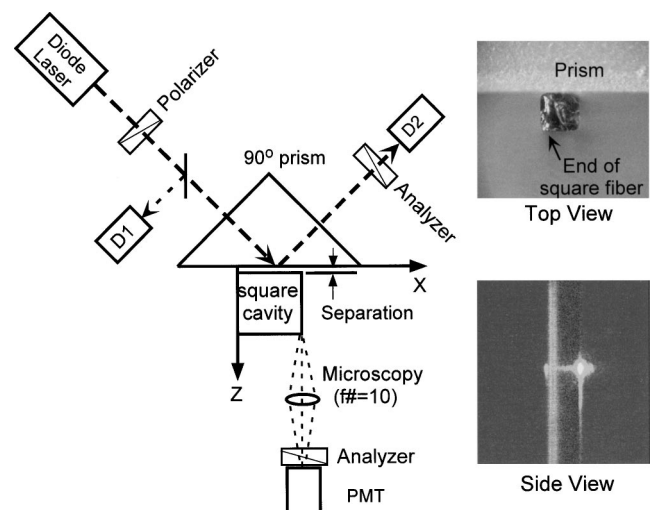


FIG. 1. Schematic of the experimental setup for measuring light coupling to a square μ cavity. *D1* and *D2* are photodiodes. PMT is a photomultiplier for detecting WGMs. The upper-right image is a microscope photograph (top view) of the prism edge and one end of the square-shaped fiber. The lower-right image is a microscope photograph (side view) of the fiber with strong emission from one edge of the fiber.

^{a)}Electronic mail: richard.chang@yale.edu

flected intensity after coupling to the square μ cavity, respectively. The prism was mounted on a mechanical stage that has all degrees of freedom. A piezoelectric extender (with 20 nm resolution) was used to change the relative prism-fiber separation. The square μ cavity is provided by a fused silica fiber (refractive index $n_3 = 1.456$) with a square cross-section ($200 \pm 3 \mu\text{m}$ edge with $\sim 30 \mu\text{m}$ radius of rounded corners). The fiber was mounted on a mechanical stage that enables the fiber to rotate along its axis (y direction) and tilt along the x or z direction. A microscope provided a top view of a portion of the prism and the adjacent fiber with a rough end (see photo at the upper right of Fig. 1). The microscope also enabled us to monitor the orientation and relative fiber-prism separation. A second microscope provided the side view (perpendicular to the prism hypotenuse) as well as transfer the light emerging from one edge of the fiber to a photomultiplier tube (PMT) with f number = 10 (see photo on the lower right of Fig. 1).

By optimizing the incident angle on the prism's hypotenuse, the orientation of the square fiber, and the prism-fiber separation, multimode resonances were observed. The upper part of Fig. 2(a) shows the remaining reflected light (from $D2$ after adjusting for maximum coupling). At WGMs, about 70% of the input intensity (for TE) has been imparted to the μ cavity. The low part of Fig. 2(a) displays the normalized-intensity spectrum of the radiation emerging from the fiber edge. For the TM case, the remaining reflected light and normalized-intensity spectrum from the fiber edge are shown in the upper and lower part of Fig. 2(b), respectively. The TM mode shows even higher energy transfer (greater than 75% at the best coupling case), but with a much broader prism-coupled WGM linewidth (lower Q value) of the resonance peaks. Both the TE and TM spectra have a free spectral range (λ_{FSR}) of 0.55 nm, which is consistent with the path length for four-bounce orbits (with $\theta_{\text{inc}} \leq 45^\circ$) of a $198.6 \mu\text{m}$ square cavity. The better external coupling with the TM WGMs is consistent with the fact that TM modes (compared with the equivalent TE modes) have longer penetration depth of the evanescent wave or higher tunneling loss through the fiber-air interface. This results in the TM WGMs having lower Q value or broader linewidth than their TE WGM counter parts.¹²

The multimode WGM spectra were investigated by varying the incident beam angle and position along the prism hypotenuse as well as the relative separation of the prism and μ cavity. By changing the input angle, the spectra from the fiber changes from that shown in Fig. 2(a) to that shown in Fig. 2(c). Although the three sets of other WGMs are detected and well resolved, only one set of WGMs is strongly coupled. The selective coupling to only one set of WGMs may be more applicable for DWDM.

The highest coupling occurs when the θ_{inc} is just larger than the θ_c of the prism as well as when the incident position is located at the middle of the square sidewall. This later phenomena is unexpected, if we assume that the same coupling for all four-bounce $\theta_{\text{inc}} = 45^\circ$ rectangular orbits at any location along the entire square edge. This discrepancy might be caused by the nonflatness of the sidewall of the square-shaped fiber. The coupling dropped when the incident position is moved away from the middle of the fiber face, where

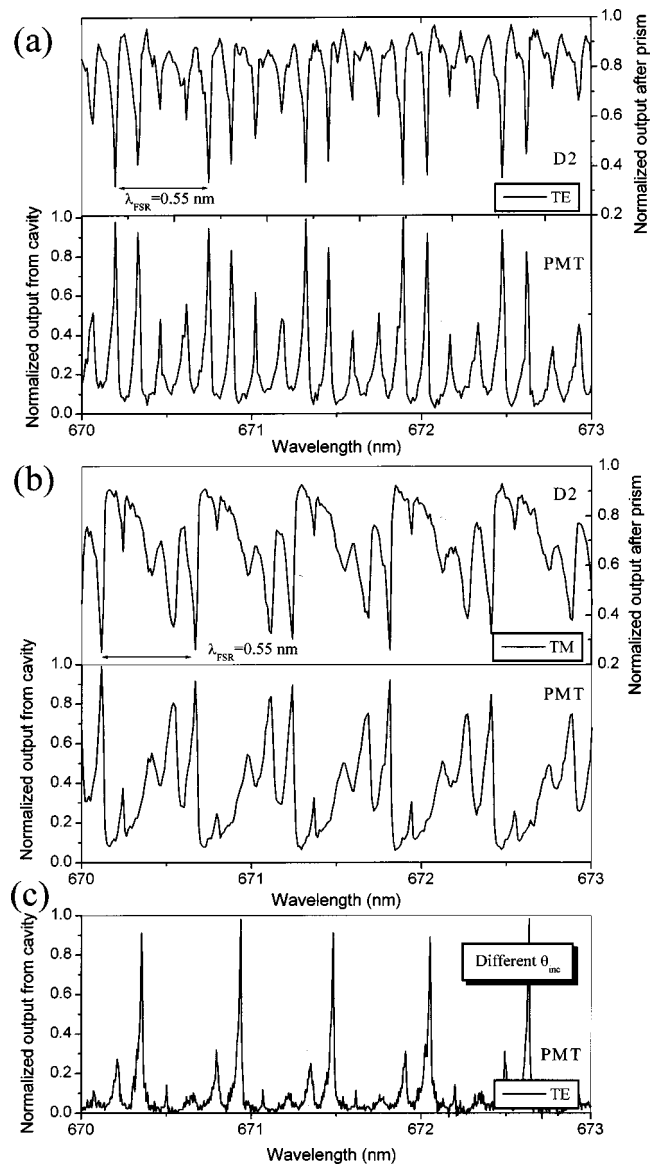


FIG. 2. (a) Upper part: normalized remaining light after coupling (TE mode), reflected by the prism and detected by $D2$. Lower part: normalized spectrum from one edge of the square-shaped μ cavity (TE modes, detected by PMT). The valleys of the upper part and the peaks of the lower part occur at the same wavelengths. (b) Upper and lower parts: same as in (a) except for TM modes. (c) Same as lower part of (a) except for a different θ_{inc} , coupling is mainly to one set of WGMs.

the separation is larger because of the roundness at the corners.

Figure 3(a) shows how sensitively the TE-WGM spectra within one free spectral range (λ_{FSR} , from 672.0 to 672.6 nm) vary with the separation around d_{mc} . The intensity of the resonance peaks decreases whether the separation is increased or decreased from d_{mc} . The linewidth of the peaks decreases (increases) when the gap is increased (decreased) from d_{mc} .

Figure 3(b) show the intensity (circle and cross symbol) and linewidth (triangle) of the TE resonance peaks at 672.38 and 672.52 nm vary with the relative separation. It indicates that different sets of WGMs have different best coupling position (or different d_{mc}), even with the same θ_{inc} . The TE modes show narrower linewidth than the TM modes and can have Q 's as high as 10^6 .

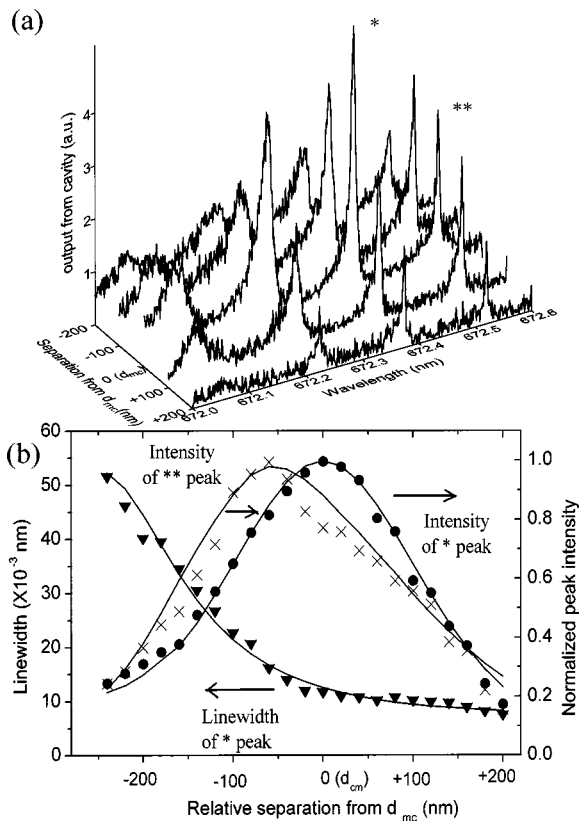


FIG. 3. (a) Spectra from one edge of the square-shaped μ cavity (TE modes) at several separations between prism and fiber. (b) The dependence of the measured linewidth (triangle) and peak intensity (circle and cross) of resonance TE peaks [marked with* and** in (a)] as a function of relative separation. The solid lines are the calculations based on assuming the square μ cavity as a Fabry-Perot resonator.

The resonance frequency, coupling efficiency, and finesse (the ratio of the separation of adjacent peaks to the half-intensity-width of the peak)¹³ of a square-like cavity (5 mm×5 mm square with the coupling face curved for confinement of resonator modes) has been derived by treating it as a standard Fabry-Perot resonator.¹⁰ These theoretical results were used to analyze our square-shaped μ cavity. The coupling efficiency $c(z)$ and finesse $F(z)$ can be expressed as

$$c(z) = \frac{[1 - \exp(-2\alpha)][1 - |\gamma(z)|^2]}{[1 - \exp(-\alpha)|\gamma(z)|]^2}, \quad (1)$$

$$F(z) = [\pi\sqrt{\exp(-\alpha)|\gamma(z)|}][1 - \exp(-\alpha)|\gamma(z)|] \quad (2)$$

because $\delta\lambda(z) = \lambda_{FSR}(z)/F(z)$, the linewidth $\delta\lambda$ of the resonance peak at different separation z can be calculated

$$\delta\lambda(z) = \frac{\lambda_{FSR}(z)[1 - \exp(-\alpha)|\gamma(z)|]}{\pi\sqrt{\exp(-\alpha)|\gamma(z)|}}, \quad (3)$$

where α is the total loss in one round-trip within the μ cavity. $\gamma(z)$ is the reflection coefficients of the wave from the μ cavity, which is dependent on the polarization, separation, and θ_{inc} . The free spectral range is λ_{FSR} . The numerical calculation of the peak intensity and linewidth of WGMs as a function of separation is shown by solid lines in Fig. 3(b). The reduced best coupling distance d_{mc} is 280 nm. The simulation results are in good agreement with the experimental data.

In conclusion, the prism coupled square μ cavity has over 75% coupling efficiency. Changing the separation between the prism and square cross-section fiber affected the WGM linewidth and coupling in accordance to a model based on Fabry-Perot resonators. By selecting the θ_{inc} , the coupling to all four sets of WGMs can be changed to couple to one set of WGMs.

The authors gratefully acknowledge the partial financial support from the Department of Energy (or Education R&D Association of Georgia University, GA0051-1), and U.S. Air Force Office of Scientific Research (F49620-00-1-0182).

- ¹ B. E. Little, S. T. Chu, W. Pan, and Y. Kokubun, *IEEE Photonics Technol. Lett.* **12**, 323 (2000).
- ² D. Rafizadeh, J. P. Zhang, S. C. Hagness, A. Taflove, K. A. Stair, and S. T. Ho, *Opt. Lett.* **22**, 1244 (1997).
- ³ V. S. Ilchenko, X. S. Yao, and L. Maleki, *Opt. Lett.* **24**, 723 (1999).
- ⁴ A. Serpenguzel, S. Arnold, G. Griffel, and J. A. Lock, *J. Opt. Soc. Am. B* **14**, 790 (1997).
- ⁵ M. Cai and K. Vahala, *Opt. Lett.* **25**, 260 (2000).
- ⁶ X. D. Fan, P. Palinginis, S. Lacey, and H. L. Wang, *Opt. Lett.* **25**, 1600 (2000).
- ⁷ J. V. Hryniewicz, P. P. Absil, B. E. Little, R. A. Wilson, and P. T. Ho, *IEEE Photonics Technol. Lett.* **12**, 320 (2000).
- ⁸ A. C. R. Pipino, J. W. Hudgens, and R. E. Huie, *Rev. Sci. Instrum.* **68**, 2978 (1997).
- ⁹ C. Manolatu, M. J. Khan, S. H. Fan, P. R. Villeneuve, H. A. Haus, and J. D. Joannopoulos, *IEEE J. Quantum Electron.* **35**, 1322 (1999).
- ¹⁰ S. Schiller, I. I. Yu, M. M. Fejer, and R. L. Byer, *Opt. Lett.* **17**, 378 (1992).
- ¹¹ A. W. Poon, F. Courvoisier, and R. K. Chang, *Opt. Lett.* **26**, 632 (2001).
- ¹² J. F. Owen, R. K. Chang, and P. W. Barker, *Opt. Lett.* **6**, 540 (1981).
- ¹³ M. Born and E. Wolf, *Principles of Optics*, 7th ed. (Cambridge University Press, Cambridge, 1999), p. 364.